



Bead-based multiplex detection of dengue biomarkers in a portable imaging device

XILONG YUAN,^{1,*}  SRISHTI GARG,¹ KEVIN DE HAAN,^{1,2} FREDERIC A. FELLOUSE,³ ANUPRIYA GOPALSAMY,³ JAN TYKVART,^{3,4} SACHDEV S. SIDHU,³ MANOJ M. VARMA,⁵ PARAMA PAL,⁶ EDITH M. HILLAN,⁷ JAMES JIAHUA DOU,⁸ AND J. STEWART AITCHISON¹

¹Department of Electrical and Computer Engineering, University of Toronto, ON, Canada

²Electrical and Computer Engineering Department, University of California at Los Angeles, Los Angeles, CA 90095, USA

³Donnelly Centre and Department of Medical Genetics, University of Toronto, ON, Canada

⁴DIANA Biotechnologies s.r.o., Vestec 252 50, Czech Republic

⁵Centre for Nano Science and Engineering, Indian Institute of Science, Bengaluru, Karnataka, India

⁶TCS Research and Innovation, Tata Consultancy Services, Bengaluru, Karnataka, India

⁷Lawrence S. Bloomberg Faculty of Nursing, University of Toronto, ON, Canada

⁸Thinkari Research Inc., Mississauga, ON, Canada

*xilong.yuan@utoronto.ca

Abstract: Dengue is one of the most rapidly spreading mosquito-borne viral diseases in the world. Differential diagnosis is a crucial step for the management of the disease and its epidemiology. Point-of-care testing of blood-borne dengue biomarkers provides an advantageous approach in many health care settings, and the ability to follow more than one biomarker at once could significantly improve the management of the disease. Bead-based multiplex technologies (suspension array) can measure multiple biomarker targets simultaneously by using recognition molecules immobilized on microsphere beads. The overarching objective of our work is to develop a portable detection device for the simultaneous measurement of multiple biomarkers important in dengue diagnosis, monitoring and treatment. Here, we present a bead-based assay for the detection of one of the four serotypes of dengue virus non-structural protein (DENV-NS1) as well as its cognate human IgG. In this system, the fluorescent microspheres containing the classification fluorophore and detection fluorophore are imaged through a microfluidic chip using an infinity-corrected microscope system. Calibration curves were plotted for median fluorescence intensity against known concentrations of DENV-NS1 protein and anti-NS1 human IgG. The limit of quantitation was 7.8 ng/mL and 15.6 ng/mL, respectively. The results of this study demonstrate the feasibility of the multiplex detection of dengue biomarkers and present its analytical performance parameters. The proposed imaging device holds potential for point-of-care testing of biomarkers on a highly portable system, and it may facilitate the diagnosis and prevention of dengue as well as other infectious diseases.

© 2020 Optical Society of America under the terms of the [OSA Open Access Publishing Agreement](#)

1. Introduction

Dengue fever is a major public health problem in tropical and sub-tropical areas. It is the fastest spreading mosquito-borne viral disease, and it affects an estimated 390 million people in more than 120 countries every year [1–3]. Dengue fever is caused by one of four antigenically distinct serotypes of dengue virus (DENV), which is a *Flavivirus* like Zika virus, West Nile virus, and yellow fever virus.

In response to the virus, infected individuals produce immunoglobins (Igs, such as IgG or IgM) against DENV envelope glycoproteins, commonly resulting in the elimination of the virus. However, in a small number of cases it evolves into a severe illness called dengue haemorrhagic

fever, which can result in life-threatening dengue shock syndrome [4]. The early or mild form of the disease shares the same symptomatic manifestation as other tropical infectious diseases, such as malaria, chikungunya, and Zika, which makes molecular testing essential for diagnosis.

The dengue non-structural protein (NS1) is present in the blood of most dengue fever infected individuals at levels that vary with time, DENV serotype, and severity of the disease. Both NS1 and the host anti-DENV IgGs and IgMs are routinely used to differentially diagnose dengue fever. However, the tests that are available commercially vary greatly in their specificity and sensitivity, and are neither quantitative nor serotype-specific [5]. Quantification of NS1, determination of the serotype at the origin of the disease, as well as monitoring of the host biomarkers could provide valuable information to guide treatment strategy and patient triage [6,7]. Hence there is a critical unmet medical need for a multiplexed diagnostic test to manage dengue fever, the principles of which would be applicable to other infectious tropical diseases.

Because NS1 and anti-NS1 IgG (thereafter, IgG) levels peak at different time over the course of the disease, the simultaneous detection of both markers enables detection throughout the disease timeline [8–11]. For example, while DENV-NS1 protein is usually found at high levels from day 1 of the onset of fever, the IgM/IgG response will typically start 3 days from the onset of fever (Fig. 1) [6].

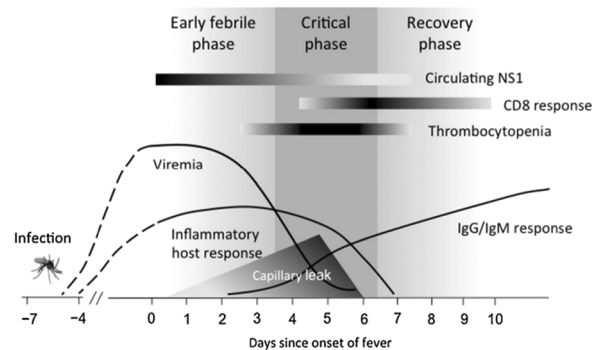


Fig. 1. Schematic showing the clinical phases in the evolution of dengue fever and its biomarkers. The figure is adapted from *Vaccine* 33, 50 (2015): 7061-7068 [6].

Point-of-care testing (POCT) holds great potential for bridging the gap between healthcare providers and patients by bringing diagnostic tests in portable and cost-effective devices right to the bedside [12]. POCT provides actionable diagnostic information at the patient's bedside without immediate need for the primary healthcare facility to have access to a medical laboratory [13–16]. Qualitative POCT platforms such as lateral flow tests are widely used, however, this approach is restricted to a positive/negative test result without the capacity to provide quantitative results. Recent technological advances, such as microfluidic sample handling, plasmon enhanced optical sensors and smartphone-based systems, enabled the development of a new generation of rapid and sensitive detection systems of biomarkers [17–22].

Compared with a single analyte assay, multiplexing can improve the throughput of biomarker detection, reduce the cost per assay by consuming less reagents/labor, and produce parallel testing results faster [23]. Bead-based multiplex immunoassays typically require the measurement of fluorescent emission using flow cytometers [24–26]. Flow cytometers can measure up to a million cells, or microspheres, in seconds and a wide range of parameters can be obtained including forward scattering, side scattering and fluorescent intensity of multiple colors. A number of lab-on-a-chip flow cytometers have been reported to measure the scattering, fluorescence and electrical impedance of different sized beads [27]. Our previous work demonstrated the capacity

of POCT for counting CD4 cells and measuring C-reactive proteins [28,29]. The success of these studies warranted the further development of a universal system for multiplex immunoassays.

The objective of this work was to develop a system capable of simultaneously detecting and quantifying DENV-NS1 protein and DENV-specific IgGs. A multiplexed and portable imaging device was prototyped using an assembly of microfluidic chips, objective lens, filters, prism, camera, etc. Monochrome images were captured to generate the fluorescence intensity values for bead set classification and biomarker detection. These data show that the system has the potential to be developed into a commercial device and fill the gap between POCT needs and the low accessibility of centralized laboratory resources.

2. Materials

2.1. Reagents and materials

Carboxyl-modified magnetic microspheres (5.5 μm) internally dyed with allophycocyanin (APC) were acquired from Spherotech Inc. (IL, USA). Serotype 1 DENV-NS1 protein was produced recombinantly as follows. Serotype 1 DENV1-NS1 cDNA from Sino Biological (cat# VG40527-G) was cloned into an in-house mammalian expression vector in frame with a C-terminal His-tag using restriction free cloning methods. HEK Expi293 cells were transiently transfected with expression plasmids using FECTO-Pro reagent (Polyplus transfection cat# 116-001) following the manufacturer's protocol. After 5 days, the cell medium was harvested and the NS1 protein purified by affinity chromatography using Ni-NTA agarose beads. A DENV-NS1-specific IgG was obtained by screening and selecting from a synthetic human antibody phage library and produced recombinantly using established methods [30], which will be described in a separate manuscript. Phycoerythrin (PE)-conjugated antibody specific to histidine chains on the NS1 protein was acquired from R&D Systems (MN, USA). Phycoerythrin-conjugated F(ab')₂ goat anti-human antibody was acquired from Jackson ImmunoResearch Laboratories (PA, USA). Coupling reagents, including N-(3-Dimethylaminopropyl)-N'-ethylcarbodiimide hydrochloride (EDC), sulfo-N-hydroxysuccinimide (sulfo-NHS), 2-(N-morpholino)ethanesulfonic acid (MES), tris(hydroxymethyl)aminomethane (Tris), hydrogen chloride (HCl), and sodium hydroxide (NaOH) were acquired from MilliporeSigma Canada Co. (ON, Canada). HCl and NaOH were used for adjusting the pH of buffer solutions. Phosphate buffer saline (PBS), Bovine serum albumin (BSA), and Tween-20 were acquired from Thermo Fisher Scientific (MA, USA).

2.2. Equipment and apparatus

The 532 nm excitation source used was a diode-pumped solid-state laser acquired from Laserglow Technologies (LRS-0532). The 635 nm excitation source was a collimated diode laser (Laserglow LRD-0635). Microfluidic chips consisting of straight channels (width, 800 μm , length 60 mm, depth 20 μm) were obtained from microfluidic ChipShop (Jena, Germany). The 10X/0.25 numerical aperture (NA) objective lens (Olympus RMS10X) and tube lens (200 mm) were acquired from Thorlabs (NJ, USA). Dual band filter FF01-577/690 was acquired from IDEX Health & Science (NY, USA). Wedge prism (#47624) was obtained from Edmund optics (NJ, USA). A Pco.edge 4.2 LT monochrome scientific camera was obtained from PCO Photonics Ltd. (ON, Canada).

3. Experimental

3.1. Bead coupling/assay

Beads encoded with different APC concentrations act as unique barcodes. The beads with high APC concentration (bead set A) were coupled with the anti-DENV-NS1 specific synthetic antibody to capture DENV-NS1 protein, while the beads with low APC concentration (bead set B) were coupled with DENV-NS1 to capture anti-DENV-NS1 IgG antibodies. Thus, as

illustrated in Fig. 2, bead set A detects the DENV-NS1 protein, while bead set B detects specific human IgGs. Carboxyl-modified beads (1 million beads) were covalently coupled with each capture protein via a two-step coupling approach [31] using magnetic separation between each step. After washing with deionized water, beads were first activated with EDC (10 mM) and sulfo-NHS (20 mM) in MES buffer (50 mM, pH 6.0) for 15 minutes. After activation, beads were washed with 200 μ L MES buffer twice. The beads were then mixed with 2.4 μ g capture protein dissolved in 200 μ L MES buffer. The mixture was incubated and mixed end-to-end for 1 hour at room temperature on a rotator. The reaction was terminated by adding 5 μ L Tris buffer (100 mM, pH 7.4). After incubation for 5 minutes, beads were washed with PBSBT (PBS, pH 7.4, 0.1% BSA (w/v), 0.05% Tween-20 (w/v)) twice. The capture beads were then resuspended in PBS to carry out the immunoassay as follows.

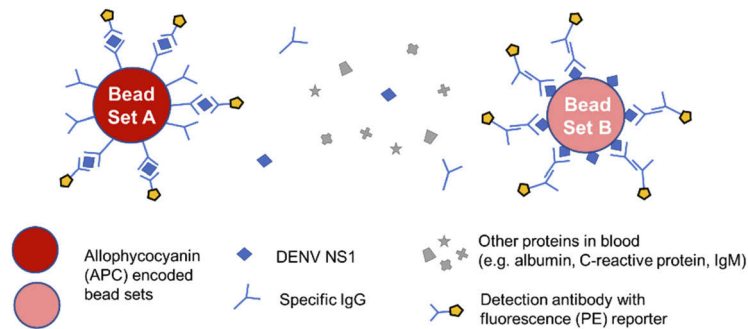


Fig. 2. Schematic of multiplex bead assay used for measuring the DENV-NS1 protein and specific IgGs in a complex sample. Bead set A contains higher concentration of APC, and bead set B contains lower concentration of APC. Bead set A captures the DENV-NS1 protein specifically, and bead set B captures specific human IgG.

A population of 50,000 capture beads was added to the individual wells of a 96-well plate (EPX-44444-000, ThermoFisher Scientific, MA, USA) and washed twice with PBST (PBS, pH 7.4; 0.05% Tween-20 (w/v)). Two-fold dilution series of DENV-NS1 standard samples were prepared in PBSB (PBS, pH 7.4; 0.1% BSA (w/v)) with concentrations ranging from 1.0 μ g/mL to 0.001 μ g/mL. The DENV-NS1 standards were mixed with capture beads in the wells and incubated for 1 hour on a plate vortex at 500 rpm at room temperature. After two washing steps with PBST using a magnetic separator, PE conjugated detection antibody was added into the beads for 30 min incubation at room temperature. The beads were then washed twice and then resuspended in PBS for detection. During the assay development process, flow cytometry was used to characterize and optimize the performance of the bead assay. After the initial characterization, beads were introduced in microfluidic channels and tested in the portable imaging device. Calibration curves of various concentrations of DENV-NS1 and IgG were plotted against the median PE fluorescent intensity. Simulated multiplex samples of DENV-NS1 and specific IgG were tested to demonstrate the characteristics of the multiplex detection.

3.2. Imaging device prototype

The optical detection system consists of a customized infinity-corrected microscope to image beads in a microfluidic chip (Fig. 3(A)). Two laser sources, with wavelengths of 532 nm and 635 nm, excite the microfluidic channel from an oblique angle of $40.7^\circ \pm 0.3^\circ$. The microfluidic chip is contained in a 3D printed cartridge, and the latter is fixed on a manual XYZ translation stage for motion control. One of the key limitations of a microfluidic-based cytometer is the potentially lower throughput, therefore limiting the number of cells or particles that can be analyzed. [32,33] To increase sample throughput we used wide (800 μ m) and shallow (20 μ m) microfluidic detection

channels. This configuration produces a ribbon-like fluid sample that increases throughput while limiting the chance of multiple beads flowing through the same location.

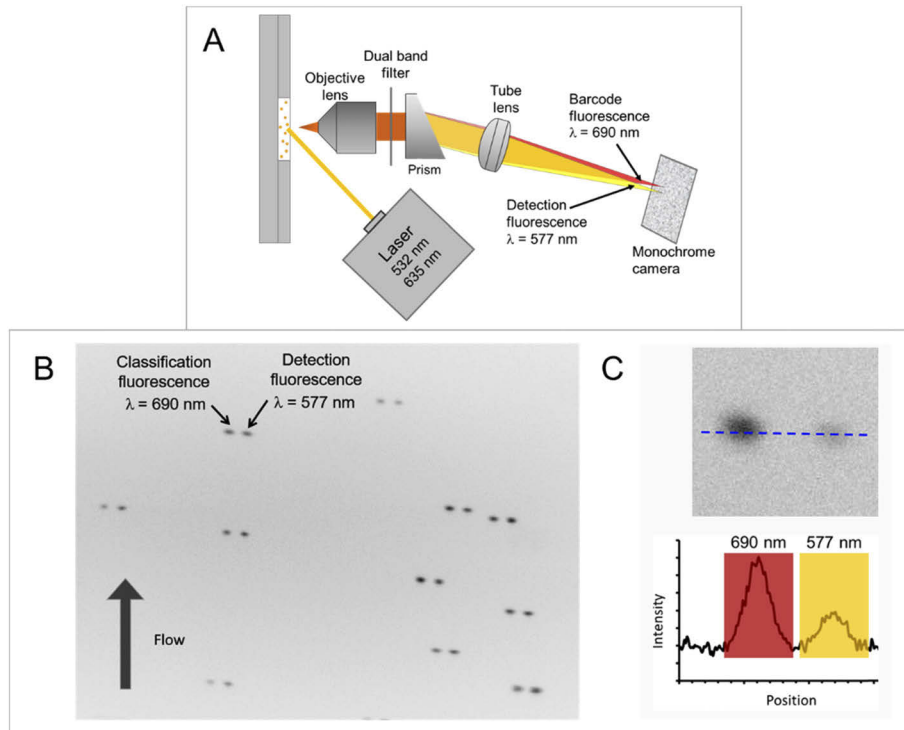


Fig. 3. A) Schematic of the infinity-corrected microscope device for imaging fluorescent microspheres in a microfluidic channel. A dual band filter and a wedge prism are used for separating the two fluorescent bands. B) An example inverted image showing the fluorescence image ‘pairs’ formed from each bead. The left band represents the classification fluorescence from APC. The right band represents the detection fluorescence from phycoerythrin. C) Schematic demonstration of the intensity profile of a bead image pair (inverted).

We adopted a prism approach to separate the two fluorescent bands. A dual bandpass filter and a prism were placed between the objective lens and tube lens (Fig. 3(A)). A dual bandpass filter was used to narrow the wavelength range of the emission bandwidth of each fluorophore and reduce the spill-over between the APC and PE fluorescence bands. Figure 3(B) shows an example of the image pairs formed after the dual band filter and the prism. Figure 3(C) shows an example of the intensity profile of the image pair. The intensity of the classification fluorescence (red) represents the identity of the bead set, indicating which biomarker is tested. The intensity of the detection fluorescence (yellow) represents the quantity of biomarkers and its intensity value correlates with the concentration of a biomarker in the fluid sample.

3.3. Image data processing

Conventional flow cytometers that use a photo multiplier tube (PMT) generate a photocurrent pulse when particles pass through the detection window. The ‘pulse’ is then amplified and converted from analog to digital values and the area, or height, value of the pulse is acquired for analysis. Here, 2048×2048 pixel images were captured by the camera. The images were analyzed using a bespoke algorithm for background subtraction, region recognition and intensity calculation.

To generate a lookup table for the pixels of the bead region of interest, the original 2D grayscale images were segmented from their background using an adaptive threshold, obtained from local first-order statistics. The local mean intensity in the neighbourhood of each pixel was used to differentiate the region of interest (ROI) pixels from total number of pixels in the image. Locally adaptive threshold uses a sensitivity factor between 0-1 range to specify sensitivity towards thresholding more pixels as foreground. The grayscale image was then converted to a binary image. The binary image was further modified to fill any empty pixels lying in the ROI, removing any connected component between bead regions. A 'regionprops' function was utilized to determine the exact number of beads in the image and their position. A pixel list of all the pixels lying in the bead region was generated and the centroid of each bead was calculated. Different approaches were evaluated to determine the 'classification' and 'detection' median fluorescence intensity (MFI) values, including measuring the height of the ROI, measuring integrated values of all ROI pixels and measuring the median grayscale value of a region around the ROI centroid [34,35]. Finally, a classification MFI was generated from integrated values of all ROI pixels. A detection MFI was generated from the median intensity value of a reduced ROI around the centroid.

After collecting the intensity values for the APC and PE channels, the first step was to define the classification (APC) fluorescence intensity range of the measured two bead sets. The second step was to statistically analyze the detection (PE) fluorescence intensity and report the MFI for the purpose of generating calibration curves and calculating sample concentrations. A logistic regression was used for curve fitting. The lower limit of quantitation (LLOQ) is defined as the lowest standard concentration showing a $\leq 20\%$ relative error between expected concentration and interpolated concentration using logistic fitting.

4. Results and discussion

4.1. Bead coupling/assay

Bead set A was coupled with a capture antibody specific to DENV-NS1, bead set B was coupled with a capture protein specific to anti-DENV-NS1 IgG. The coupling efficiency was confirmed by performing a bead-based enzyme-linked immunosorbent assay using serial dilutions of the target protein. It was found that Tween-20 interferes with the coupling reaction and reduced the surface coverage of the capture proteins significantly. Tween-20 was therefore avoided in the activation and coupling reactions and the washing steps. However, after bead coupling, we found that the PBST suspension buffer had a higher bead count recovery than PBS because Tween-20 reduced the attachment of beads to the tube surface. Coupled beads were then analyzed by measuring forward scattering, side scattering, and APC fluorescence intensity in a flow cytometer before and after coupling. Forward scattering, side scattering and APC intensity had less than a 3.0% change after the coupling reaction. This indicated that the bead diameter, surface morphology and internal APC concentration remained consistent after coupling.

The number of beads required for imaging in the microfluidic channel was estimated based on the dimension of the channel and imaging frame. For example, approximately 25,000 beads were required in a 10 μL sample, according to the dimension of the microfluidic channel ($W \times D \times L$: $0.80 \times 0.020 \times 58.5$ mm), an assumed imaging frame (0.5×0.5 mm) and an assumed concentration of 10 beads per frame. Accounting for the possible loss of beads along the immunoassay and transfer, 50,000 coupled beads were used to perform the immunoassay. Twenty percent of the bead population was analyzed by flow cytometry as a reference and the rest of sample was analyzed in the imaging device. Four-parameter logistic (4PL) regression curves were plotted for varying concentrations of DENV-NS1 and IgG proteins ranging from 0.001 $\mu\text{g/mL}$ to 1.0 $\mu\text{g/mL}$. The percentage error of the expected concentration and the interpolated concentration (from 4PL curves using flow cytometer results) was used to evaluate the performance of the bead assay itself. Flow cytometry results showed that the percentage error was less than 5%

for concentration levels from 0.004 to 1.0 $\mu\text{g/mL}$. This indicated that the current immunoassay could accurately measure the quantity of DENV-NS1 and IgG in the range of 0.004 to 1.0 $\mu\text{g/mL}$ using flow cytometry. Further investigation of the proposed imaging device was performed and is discussed in the following sections.

4.2. Device prototyping

Because of the wavelength difference between the fluorescence bands used, 565-589 nm (center wavelength 577 nm) and 665-715 nm (center wavelength 690 nm), a 15° prism was used to separate the two bands with a 0.078° angular deviation. Considering the angle and distance from the prism to the camera sensor, a separation of 55.7 pixels should be achieved at the imaging sensor. The 565-589 nm band presented a 15-pixel dispersion on the image plane, and the 665-715 nm band caused 19.5 pixels of dispersion. However, due to differing levels of focus being achieved throughout the channel, the pixel gap between the two bands was smaller in practice. As shown in Fig. 3(B), the separation between the two images in a bead pair ranged from 20-25 pixels (based on peak width at 5% peak height) and this was dependent on the intensity of both bands.

The red laser was utilized to excite the internal classification fluorescent dye (APC), and the green laser was used to excite the labelled detection fluorescent dye (PE). The excitation power was calibrated with a power meter to supply a consistent power level of 30 mW for the green laser and 45 mW for the red laser. Because of the Gaussian distribution of the beam intensity, it remained a challenge to maintain a uniform beam profile across the entire frame. After characterizing the beam size and intensity distribution, an elliptical area 480×720 pixels (minor axis \times major axis) was used for further analysis. Within this area, the beam intensity varied by less than 10%. This area corresponded to a $240 \times 360 \mu\text{m}$ (minor axis \times major axis) elliptical area on the microfluidic channel.

In order to maximize the sensor area used to image the flow channel, while ensuring a sufficient depth of field (DOF), a 10x/0.25 numerical aperture (NA) objective lens was chosen. The DOF for this lens was smaller than the depth of the channel. However, as the intensity of the entire bead was measured, the focus was sufficient throughout the channel using this objective. While using a higher resolution 20x/0.4 NA objective lens (Olympus RMS20X) was tested to improve image resolution, that lens had a smaller DOF and the beads became highly out of focus when they were imaged at the edges of the channel. Therefore, the 10x/0.25 NA objective lens was used for further experiments to match with the width of the microfluidic channel and to generate the highest quality images of the fluorescent beads.

Two technical approaches were utilized to capture images of microspheres, the static-chip approach, and the static-fluid approach. The static-chip approach requires the pumping of fluids in microfluidic channels and the microfluidic chip assembly does not move. This approach captures images through a fixed area of the microfluidic channel. Therefore, once the imaging plane is in focus, it does not require further refocusing and will image the fluorescent bead at a higher speed. However, the flow velocity of microspheres in fluids must be carefully controlled to maintain the quality of images. Because consistent bead motion is required while capturing images, the effects of viscous force, inertial force and pressure change must be characterized and compensated for different fluid samples. Experiments were performed to image the flowing beads in microfluidic channels, but it was observed that the static-chip approach required a significant amount of high bead concentration sample to generate sufficient bead images for further analysis. Therefore, another approach, the static-fluid approach was attempted since it requires the fluid to be fixed/motionless in the channel when the camera sensor captures images. Because the precise control of bead flow is not required, this approach could accommodate various fluid sample types without the need to optimize the fluidic control system. To capture enough image frames, a longer microfluidic channel may be required, and the microfluidic chip assembly may

be motorized to acquire multiple images. To test the feasibility of the static-fluid approach, we utilized a microfluidic chip with long channels (length 60 mm) and multiple images were captured by manually moving the microfluidic chip along the channel. The captured image sets were then used for intensity analysis.

4.3. Bead classification

The classification capability of the proposed device was characterized using an array of bead sets with four levels of classification intensity. Flow cytometry was first performed to evaluate the distribution of classification intensities. The coefficient of variation of each bead set fluorescence intensity was in the range of 7.7-10.8%. The same sample was measured through the imaging device and the coefficient of variation was in the range of 12.0-23.1%. This demonstrated the capability of the imaging device for measuring four bead sets at once, although the higher coefficient of variation compared with the flow cytometer is attributed to laser intensity fluctuation across the frame and clumping of multiple beads to form doublets or triplets. Different laser excitation power levels (15, 30, 45 mW) were tested to effectively separate the four intensity peaks. An incident power 45 mW provided the best performance for classifying the tested APC intensities. Two bead sets were used to perform the bead coupling and immunoassay as described in section 4.1.

4.4. Calibration curves

The imaging device was used to measure standard samples with varying concentrations of DENV-NS1 and IgG. Calibration curves were plotted by analyzing the detection intensity of bead images (Fig. 3(B)). As shown in Fig. 4 and 5, the expected correlation between the median fluorescence intensity and the concentration was observed. 4PL regression was used to fit the detection fluorescence intensity with the expected standard concentrations. The DENV-NS1 and IgG assays were able to measure a relatively low concentration in both samples, with the lower limit of quantitation at 7.8 ng/mL and 15.6 ng/mL respectively. These concentration levels are significantly lower than clinically relevant concentrations of DENV-NS1 and IgG proteins, and they are comparable to the assay range of conventional ELISA methods [9,11,36].

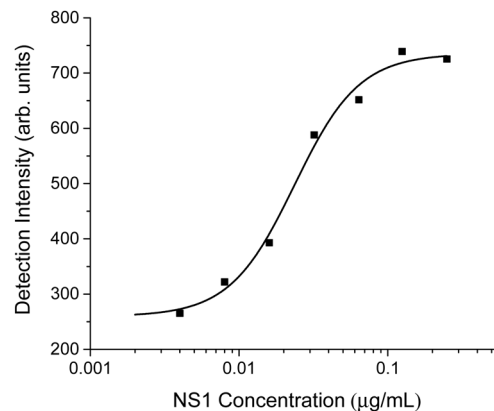


Fig. 4. Calibration curves of DENV-NS1 protein at concentrations of 0.004 - 1.0 µg/mL against the median fluorescence intensity of the detection band centered at 577 nm. Curves are fitted with 4PL regression ($R^2 = 0.99$). Standard deviations of detection intensity of individual beads range from 101.5-141.1.

Comparably, bead intensity for the IgG assay had a higher standard deviation than for the DENV-NS1 assay, presumably resulting from the less uniform coverage of the capture protein.

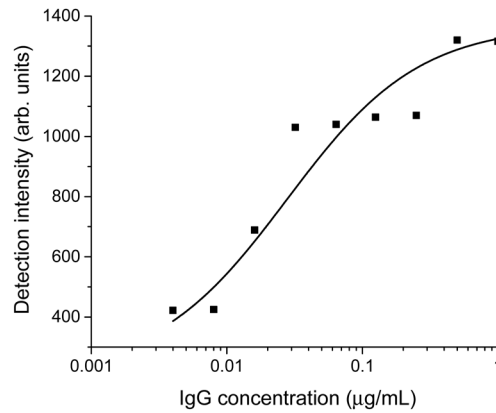


Fig. 5. Calibration curves of IgG at concentration of 0.004 - 1.0 µg/mL against the median fluorescence intensity of the detection band centered at 577 nm. Curves are fitted with 4PL regression ($R^2 = 0.93$). Standard deviations of detection intensity of the individual concentration level range from 178.6-337.9.

This leads to a higher standard deviation of detection intensity of beads either in flow cytometry or in imaging device measurements. To improve the uniformity of the capture reagent coverage on beads, additional coupling protocols should be investigated, especially with the mixing/handling procedures and chemical compositions (buffer composition, pH). It was observed that end-to-end mixing of the coupling reaction is important for achieving a more uniform distribution of surface protein coverage, presumably due to reduced aggregation and absorption of beads on the centrifuge tube wall. Surfactants (e.g. Tween-20) could potentially alleviate this issue although it may interfere with the efficiency of coupling reaction. Therefore, further investigation may be required to develop the optimal protocols for the coupling reaction.

4.5. Multiplex sample

Effective quantitation of multiple biomarkers could help diagnose the phase of dengue infection. To demonstrate the concept of multiplex detection, bead-based assays for DENV-NS1 and IgG were performed separately in microcentrifuge tubes. The bead samples from these two assays were mixed in different combinations to simulate an actual sample measurement [1,3,6,37]. Shown in Fig. 6 are scatter plots for the individual events detected using the imaging device. Simulated multiplex samples of the DENV-NS1 assay and the IgG assay at various concentration levels were measured. Cut-off values of classification intensity were applied to the DENV-NS1 assay (280-360) and the IgG assay (145-225). Some events were detected between the classified bead sets or beyond a normal intensity range. This is potentially due to the aggregation of beads to form doublets, triplets, etc. For a typical multiplex assay in flow cytometry, at least 35-50 events are required for each bead set to generate statistically significant measurements [38,39]. The current study adopted the similar strategy of maintaining at least 35 events per single assay. It was considered that the two bead samples may agglutinate with each other because of the complementary antibody affinity. However, this was not observed in the performed bead detection experiments. Theoretically, agglutination happens preferably among much smaller microspheres (<1,000 nm). Additionally, clumps of larger microspheres may not be strong enough to withstand the hydrodynamic forces trying to break them apart, and it will take considerably longer for all the larger microspheres to form clumps [40].

According to previous research, circulating DENV-NS1 ranges from 7 to 280 ng/mL in dengue-positive patients' sera [11]. Another study showed that free DENV-NS1 levels in plasma

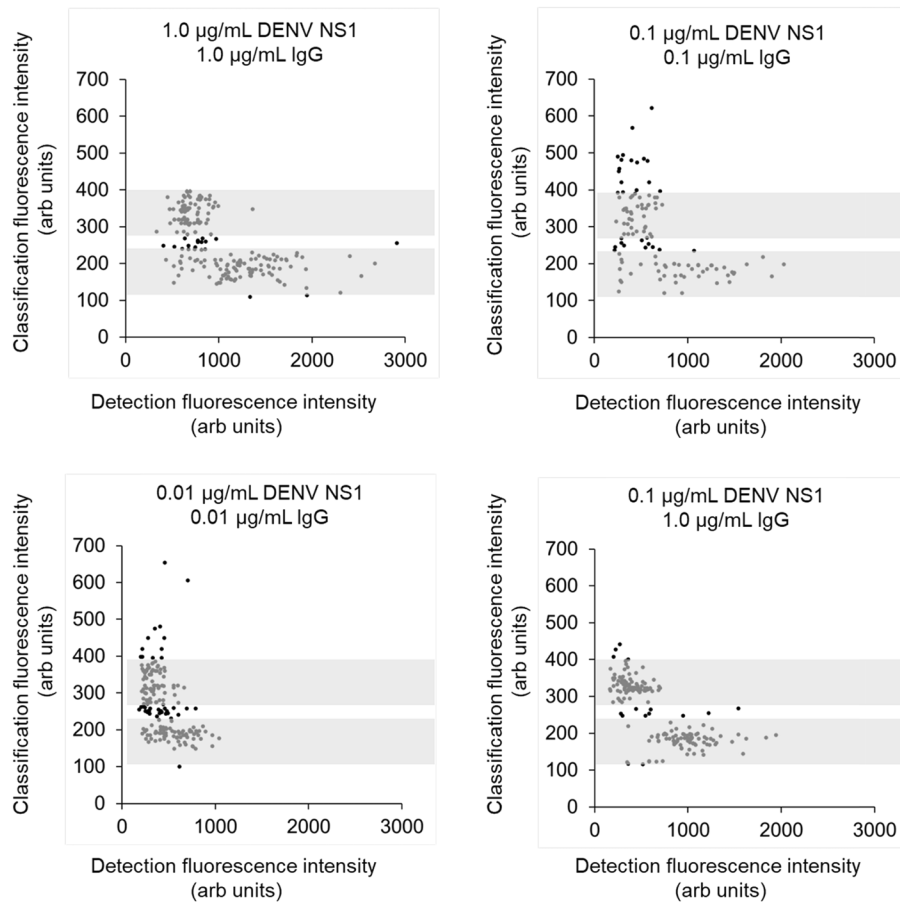


Fig. 6. Scatter plots of the classification fluorescence intensity (y) versus the detection fluorescence intensity (x) for multiplex assays of various concentration combinations of DENV-NS1 and IgG. The upper gray bar represents the classification cut-off intensity for DENV-NS1 assay. The lower gray bar represents the classification cut-off intensity for IgG assay.

correlated with viremia levels and were higher in patients with dengue hemorrhagic fever than in those with dengue fever. An elevated serum DENV-NS1 level (≥ 600 ng/mL) within 72 h of illness onset identified patients at risk for developing dengue hemorrhagic fever [41]. Therefore, the detection range in our detection system has the potential to accommodate the DENV-NS1 sensitivity requirements for patient samples. Quantitative ELISA is usually performed using a designated positive serum calibrator from infected patients [42]. Optical density ratios between the designated calibrator and the specimen are used as 'quantitative' values, but this does not give a molar or mass concentration amount for any pathogen or epitope-specific IgG. Here, in contrast, a specific IgG is used as the calibrator. This will require testing a set of positive calibrator and negative control samples to properly calibrate the concentration of specific IgG standards with the antibody titer in clinical samples. Previous research showed that epitope-specific IgG concentrations ranged from 0.4 to 21 $\mu\text{g/mL}$ for a bacterial infection [43]. Our detection system can quantify specific IgG as low as 0.0156 $\mu\text{g/mL}$, and therefore, it will enable sensitive detection of specific IgG. Its analytical performance, such as linearity and interference, needs to be further studied, however, our detection systems provides a new tool to investigate the antibody titers of

positive calibrator sera and it holds strong potential to be developed and deployed for clinical validation.

4.6. Discussion

One important aspect for a field deployable diagnostic device is the shelf-life of the reagents. This is influenced by two factors: the stability of the coupled beads and the longevity of the pre-packaged, microfluidic device containing the assay reagents. First, the stability of the coupled beads will depend on the nature of the coupling reaction, such as covalent bond coverage and non-specific absorption coverage. According to specifications of typical off-the-shelf bead-based assay reagents, the coupled beads could last for 12 months, or longer when they are stored under proper conditions (e.g. 2-8 °C in buffer solutions containing a stabilizer and preservatives) [44]. Second, if the reagents can be freeze-dried, or air-dried and immobilized in the microfluidic cartridge, the prefabricated testing cartridge may not need to be stored in a refrigerator. Room-temperature storage may be feasible and therefore, its distribution facilitated. Ultimately, the stability of the beads and testing cartridges require the tracking of their analytical performance over time and these experiments are currently underway.

The repeatability of the presented biosensing method can be approached by analyzing the coefficient of variation of obtained analyte concentration between repeated image capturing. The CV% is determined to be 22.6% for the NS1 and 33.9% for the specific IgG at a respective concentration level of 0.01 µg/mL. It should be noted that this repeatability value can be further improved by optimizing the bead coupling protocol and applying a more uniform laser illumination source. Another factor that may contribute to the repeatability of the measurement is the photostability of the reporter fluorophore, PE. Also, labeling the beads with more durable reporter fluorophore (e.g. Quantum dots) may in theory improve the measurement precision. Overall, we have demonstrated the feasibility of the biosensing method and we have devised a strategy to further improve its performance.

In this study, APC is used for classification fluorescence, and PE is used for detection fluorescence. The selection of these two dyes is based on the availability of off-the-shelf fluorescent microspheres and fluorescent labels for flow cytometry applications. PE is widely used in flow cytometry detection because it has a very high quantum yield and therefore permits higher sensitivity. However, it was observed that PE brightness decreases within seconds when illuminated at a power of 50 mW, due to its susceptibility to photobleaching. This is not a concern for flow cytometry because individual beads pass through the detection window within microseconds [45]. But it emphasizes the need for the imaging device to interrogate the beads and capture images within a very short period (seconds) to counteract the photobleaching of PE. Therefore, the camera must be set to a short exposure time. Alternatively, other fluorophores could be considered. For example, quantum dot (QD) 565 was tested in the current set-up, and the brightness of QD565 was relatively low compared to PE, because of the low excitation efficiency of 532 nm for QD565. By replacing the 532 nm laser with a 405 nm laser, the excitation efficiency of quantum dots may be significantly improved.

The proposed device demonstrates the potential for measuring multiple biomarkers in a miniaturized setting. Oblique illumination was adopted in the current prototype for simplicity. Epifluorescence could be better for improving sensitivity by preventing the diffuse stray light reaching the detector. Image processing algorithms were successfully applied for the classification and detection of fluorescent beads. Further developments may involve intensity normalization using blank control beads and classification beads. Doublet beads may be present in the samples, requiring an event screening using morphology factors in addition to the intensity-based classification, akin to the singlet gating operation (forward scattering/side scattering) used in flow cytometer. The biosensing system presented is applicable to the detection of large protein molecules (e.g. > 10 kD) and the assay system should be capable of detecting

other virus antigens based on the principle of sandwich immunoassay. Therefore, it holds great potential to be developed into a point-of-care testing device for the detection of dengue and other infectious diseases.

5. Conclusions

This proof-of-concept study was performed to demonstrate the characteristics of a new imaging device built to detect one of the serotypes of DENV-NS1 and the corresponding specific IgG antibody in a multiplex bead assay. Fluorescence intensity was calibrated with known concentration of the target DENV-NS1 and IgG. The lower limit of quantitation was shown to meet the reference range requirements for clinical samples and further investigation is needed to validate the analytical performance in clinical positive and negative specimens. This imaging device makes an important contribution to the development of a fully functional POCT device for the diagnosis of dengue fever and other emerging infectious diseases.

Funding

IC-IMPACTS (the India-Canada Centre for Innovative Multidisciplinary Partnerships to Accelerate Community Transformation and Sustainability).

Acknowledgments

The authors acknowledge the support from IC-IMPACTs and the Government of Ontario.

The project is funded by IC-IMPACTS (the India-Canada Centre for Innovative Multidisciplinary Partnerships to Accelerate Community Transformation and Sustainability).

Disclosures

The authors declare no conflicts of interest.

References

1. N. T. Darwish, S. D. Sekaran, and S. M. Khor, "Point-of-care tests: a review of advances in the emerging diagnostic tools for dengue virus infection," *Sens. Actuators, B* **255**, 3316–3331 (2018).
2. D. Normile, "Surprising New Dengue Virus Throws a Spanner in Disease Control Efforts," *Science* **342**(6157), 415 (2013).
3. J. Pang, P. Y. Chia, D. C. Lye, and Y. S. Leo, "Progress and Challenges towards Point-of-Care Diagnostic Development for Dengue," *J. Clin. Microbiol.* **55**(12), 3339–3349 (2017).
4. "Dengue: guidelines for diagnosis, treatment, prevention and control," (World Health Organization, 2009).
5. H. Lee, J. H. Ryu, H. S. Park, K. H. Park, H. Bae, S. Yun, A. R. Choi, S. Y. Cho, C. Park, D. G. Lee, J. Lim, J. Lee, S. Lee, S. Shin, H. Park, and E. J. Oh, "Comparison of Six Commercial Diagnostic Tests for the Detection of Dengue Virus Non-Structural-1 Antigen and IgM/IgG Antibodies," *Ann. Lab. Med.* **39**(6), 566–571 (2019).
6. C. P. Simmons, K. McPherson, N. Van Vinh Chau, D. T. Hoai Tam, P. Young, J. Mackenzie, and B. Wills, "Recent advances in dengue pathogenesis and clinical management," *Vaccine* **33**(50), 7061–7068 (2015).
7. A. L. Conroy, M. Gelvez, M. Hawkes, N. Rajwans, V. Tran, W. C. Liles, L. A. Villar-Centeno, and K. C. Kain, "Host biomarkers are associated with progression to dengue haemorrhagic fever: a nested case-control study," *Int. J. Infect. Dis.* **40**, 45–53 (2015).
8. P. Koraka, C. P. Burghoorn-Maas, A. Falconar, T. E. Setiati, K. Djamiatun, J. Groen, and A. D. Osterhaus, "Detection of immune-complex-dissociated nonstructural-1 antigen in patients with acute dengue virus infections," *J. Clin. Microbiol.* **41**(9), 4154–4159 (2003).
9. S. M. Wang and S. D. Sekaran, "Early Diagnosis of Dengue Infection Using a Commercial Dengue Duo Rapid Test Kit for the Detection of NS1, IGM, and IGG," *Am. J. Trop. Med. Hyg.* **83**(3), 690–695 (2010).
10. S. D. Blacksell, R. G. Jarman, M. S. Bailey, A. Tanganuchitcharnchai, K. Jenjaroen, R. V. Gibbons, D. H. Paris, R. Premaratna, H. J. de Silva, D. G. Lalloo, and N. P. Day, "Evaluation of six commercial point-of-care tests for diagnosis of acute dengue infections: the need for combining NS1 antigen and IgM/IgG antibody detection to achieve acceptable levels of accuracy," *Clin. Vaccine Immunol.* **18**(12), 2095–2101 (2011).
11. D. Allonso, M. D. Meneses, C. A. Fernandes, D. F. Ferreira, and R. Mohana-Borges, "Assessing positivity and circulating levels of NS1 in samples from a 2012 dengue outbreak in Rio de Janeiro, Brazil," *PLoS One* **9**(11), e113634 (2014).

12. I. Hernández-Neuta, F. Neumann, J. Brightmeyer, T. Ba Tis, N. Madaboosi, Q. Wei, A. Ozcan, and M. Nilsson, "Smartphone-based clinical diagnostics: towards democratization of evidence-based health care," *J. Intern. Med.* **285**(1), 19–39 (2019).
13. R. Wang, S. Y. Ongagna-Yhombi, Z. Lu, E. Centeno-Tablante, S. Colt, X. Cao, Y. Ren, W. B. Cardenas, S. Mehta, and D. Erickson, "Rapid Diagnostic Platform for Colorimetric Differential Detection of Dengue and Chikungunya Viral Infections," *Anal. Chem.* **91**(8), 5415–5423 (2019).
14. H. Ye and X. Xia, "Enhancing the sensitivity of colorimetric lateral flow assay (CLFA) through signal amplification techniques," *J. Mater. Chem. B* **6**(44), 7102–7111 (2018).
15. T. R. Kozel and A. R. Burnham-Marusich, "Point-of-Care Testing for Infectious Diseases: Past, Present, and Future," *J. Clin. Microbiol.* **55**(8), 2313–2320 (2017).
16. T. Oeschger, D. McCloskey, V. Koppa, A. Singh, and D. Erickson, "Point of care technologies for sepsis diagnosis and treatment," *Lab. Chip.* **19**(5), 728–737 (2019).
17. A. Ahmadvand, B. Gerislioglu, P. Manickam, A. Kaushik, S. Bhansali, M. Nair, and N. Pala, "Rapid Detection of Infectious Envelope Proteins by Magnetoplasmonic Toroidal Metasensors," *ACS Sens.* **2**(9), 1359–1368 (2017).
18. A. Ahmadvand, B. Gerislioglu, A. Tomitaka, P. Manickam, A. Kaushik, S. Bhansali, M. Nair, and N. Pala, "Extreme sensitive metasensor for targeted biomarkers identification using colloidal nanoparticles-integrated plasmonic unit cells," *Biomed. Opt. Express* **9**(2), 373–386 (2018).
19. H. Zhu, S. Mavandadi, A. F. Coskun, O. Yaglidere, and A. Ozcan, "Optofluidic fluorescent imaging cytometry on a cell phone," *Anal. Chem.* **83**(17), 6641–6647 (2011).
20. Y. Rivenson, H. Ceylan Koydemir, H. Wang, Z. Wei, Z. Ren, H. Günaydın, Y. Zhang, Z. Gorocs, K. Liang, and D. Tseng, "Deep learning enhanced mobile-phone microscopy," *ACS Photonics* **5**(6), 2354–2364 (2018).
21. C. Vietz, M. L. Schutte, Q. Wei, L. Richter, B. Lalkens, A. Ozcan, P. Tinnefeld, and G. P. Acuna, "Benchmarking Smartphone Fluorescence-Based Microscopy with DNA Origami Nanobeads: Reducing the Gap toward Single-Molecule Sensitivity," *ACS Omega* **4**(1), 637–642 (2019).
22. J. W. Snow, H. C. Koydemir, D. K. Karınca, K. Liang, D. Tseng, and A. Ozcan, "Rapid imaging, detection, and quantification of *Nosema ceranae* spores in honey bees using mobile phone-based fluorescence microscopy," *Lab. Chip.* **19**(5), 789–797 (2019).
23. Y. Leng, K. Sun, X. Chen, and W. Li, "Suspension arrays based on nanoparticle-encoded microspheres for high-throughput multiplexed detection," *Chem. Soc. Rev.* **44**(15), 5552–5595 (2015).
24. H. Graham, D. J. Chandler, and S. A. Dunbar, "The genesis and evolution of bead-based multiplexing," *Methods* **158**, 2–11 (2019).
25. C. Dincer, R. Bruch, A. Kling, P. S. Dittrich, and G. A. Urban, "Multiplexed point-of-care testing—xPOCT," *Trends Biotechnol.* **35**(8), 728–742 (2017).
26. J. Rho, W. Jang, I. Hwang, D. Lee, C. H. Lee, and T. D. Chung, "Multiplex immunoassays using virus-tethered gold microspheres by DC impedance-based flow cytometry," *Biosens. Bioelectron.* **102**, 121–128 (2018).
27. E. Morgan, R. Varro, H. Sepulveda, J. A. Ember, J. Apgar, J. Wilson, L. Lowe, R. Chen, L. Shivraj, and A. Agadir, "Cytometric bead array: a multiplexed assay platform with applications in various areas of biology," *Clin. Immunol. (Amsterdam, Neth.)* **110**(3), 252–266 (2004).
28. J. J. Dou, J. S. Aitchison, L. Chen, and R. Nayyar, "Portable point-of-care blood analysis system for global health," in *SPIE BiOS: Optics and Biophotonics in Low-Resource Settings II* (International Society for Optics and Photonics 2016), p. 96990M.
29. S. Jagadeesh, L. Chen, and S. Aitchison, "Fluorescent detection of C-reactive protein using polyamide beads," in *SPIE BiOS: Optical Diagnostics and Sensing XVI: Toward Point-of-Care Diagnostics* (International Society for Optics and Photonics 2016), p. 971505.
30. F. A. Fellouse, K. Esaki, S. Birtalan, D. Raptis, V. J. Cancasci, A. Koide, P. Jhurani, M. Vasser, C. Wiesmann, A. A. Kossiakoff, S. Koide, and S. S. Sidhu, "High-throughput generation of synthetic antibodies from highly functional minimalist phage-displayed libraries," *J. Mol. Biol.* **373**(4), 924–940 (2007).
31. W. Kong, C. Xiao, G. Ying, X. Liu, X. Zhao, R. Wang, L. Wan, and M. Yang, "Magnetic microspheres-based cytometric bead array assay for highly sensitive detection of ochratoxin A," *Biosens. Bioelectron.* **94**, 420–428 (2017).
32. A. B. Shrirao, Z. Fritz, E. M. Novik, G. M. Yarmush, R. S. Schloss, J. D. Zahn, and M. L. Yarmush, "Microfluidic flow cytometry: The role of microfabrication methodologies, performance and functional specification," *Technology* **6**(1), 1–23 (2018).
33. S. Y. Yang, K. Y. Lien, K. J. Huang, H. Y. Lei, and G. B. Lee, "Micro flow cytometry utilizing a magnetic bead-based immunoassay for rapid virus detection," *Biosens. Bioelectron.* **24**(4), 855–862 (2008).
34. S. Garg, "A Multiplexed, Point-of-Care Detection System for Dengue," in *Department of Electrical and Computer Engineering* (University of Toronto, 2019).
35. S. Garg, R. X. Yuan, A. Gopalsamy, F. A. Fellouse, S. S. Sidhu, J. Dou, and J. S. Aitchison, "A Multiplexed, Point-of-Care Sensing for Dengue," in *2019 IEEE SENSORS* (2019), pp. 1–4.
36. S. Alcon, A. Talarmin, M. Debryne, A. Falconar, V. Deubel, and M. Flamand, "Enzyme-linked immunosorbent assay specific to Dengue virus type 1 nonstructural protein NS1 reveals circulation of the antigen in the blood during the acute phase of disease in patients experiencing primary or secondary infections," *J. Clin. Microbiol.* **40**(2), 376–381 (2002).

37. S. M. Wang and S. D. Sekaran, "Early diagnosis of Dengue infection using a commercial Dengue Duo rapid test kit for the detection of NS1, IGM, and IGG," *Am. J. Trop. Med. Hyg.* **83**(3), 690–695 (2010).
38. "Bio-Plex Pro™ Human Cytokine Screening Panel, Instruction Manual," <https://www.bio-rad.com/webroot/web/pdf/lsr/literature/10000092045.pdf>.
39. MilliporeSigma, "Tips and Tricks: The Power of Multiplex Biomarker Analysis from the makers of MILLIPLEX® map," https://www.sigmaaldrich.com/content/dam/sigma-aldrich/docs/Sigma-Aldrich/Brochure/1/br1088en_ms.pdf.
40. "Immunological Application by Bangs Laboratories Inc.," <https://www.bangslabs.com/sites/default/files/imce/docs/TechNote%20301%20Web.pdf>.
41. D. H. Libraty, P. R. Young, D. Pickering, T. P. Endy, S. Kalayanaraj, S. Green, D. W. Vaughn, A. Nisalak, F. A. Ennis, and A. L. Rothman, "High circulating levels of the dengue virus nonstructural protein NS1 early in dengue illness correlate with the development of dengue hemorrhagic fever," *J. Infect. Dis.* **186**(8), 1165–1168 (2002).
42. "Dengue Virus IgG DxSelect," <https://www.focusdx.com/pdfs/pi/OUS/EL1500G-OUS.pdf>.
43. A. Soininen, I. Seppala, T. Wuorimaa, and H. Kayhty, "Assignment of immunoglobulin G1 and G2 concentrations to pneumococcal capsular polysaccharides 3, 6B, 14, 19F, and 23F in pneumococcal reference serum 89-SF," *Clin. Diagn. Lab. Immunol.* **5**(4), 561–566 (1998).
44. "CRP Human ProcartaPlex™ Simplex Kit (certificate of analysis)," <https://www.thermofisher.com/order/catalog/product/EPX01A-10288-901#EPX01A-10288-901>.
45. Y. Han, Y. Gu, A. C. Zhang, and Y. H. Lo, "Review: imaging technologies for flow cytometry," *Lab. Chip.* **16**(24), 4639–4647 (2016).